

Influence of electron-phonon scattering for an on-demand quantum dot single-photon source using cavity-assisted adiabatic passage

Chris Gustin* and Stephen Hughes

Department of Physics, Engineering Physics and Astronomy, Queen's University, Kingston, Ontario, Canada K7L 3N6
(Received 22 June 2017; revised manuscript received 19 July 2017; published 10 August 2017)

We study the role of electron-phonon scattering for a pulse-triggered quantum dot single-photon source which utilizes a modified version of stimulated Raman adiabatic passage and cavity coupling. This on-demand source is coherently pumped with an optical pulse in the presence of a continuous-wave laser drive, allowing for efficient generation of indistinguishable single photons with polarizations orthogonal to the applied fields. In contrast to previous studies, we explore the role of electron-phonon scattering on this semiconductor system by using a polaron master equation approach to model the biexciton-exciton cascade and cavity mode coupling. In addition to background zero-phonon-line decoherence processes, microscopic electron-acoustic-phonon coupling, which usually degrades the indistinguishability and efficiency of semiconductor photon sources, is rigorously taken into account. We study how different system parameters (including cavity and laser detunings, cavity spectral width, temperature) affect the device performance and contrast the relative influence of intrinsic phonon coupling with other dephasing mechanisms. We describe how this biexciton-exciton cascade scheme allows for true single photons to be generated with over 90% quantum indistinguishability and efficiency simultaneously using realistic experimental parameters. We also show how the double-field dressing can be probed through the cavity-emitted spectrum.

DOI: [10.1103/PhysRevB.96.085305](https://doi.org/10.1103/PhysRevB.96.085305)

I. INTRODUCTION

Integral to many schemes of quantum information processing, including linear quantum computation [1] and quantum cryptography [2], is a deterministic source of on-demand single photons. Effective on-demand single-photon sources are efficient quantum light sources (emitting a single photon each time they are triggered) which produce photons that can be indistinguishable in frequency, polarization, and bandwidth. In practical sources, these important figures of merit are degraded by decoherence arising from the source coupling to its environment, typically containing a large number of quantum degrees of freedom. Decoherence (particularly optical dephasing in semiconductor structures) has proven to be a substantial barrier to practical implementation of nanotechnology which incorporates quantum-mechanical phenomena [3–5]. However, some of these barriers are not necessarily fundamental ones, and methods exist and are improving which can reduce decoherence in semiconductor single-photon sources [6–8].

Nanoscale semiconductor quantum dots (QDs) function as solid-state “artificial atoms” and are promising candidates for scalable single-photon sources [9,10]. The presence of an electronic band gap allows for an optically active transition between ground and spatially confined excited electron-hole pair (exciton) states, mimicking a two- (or more) level atom, but with notable advantages including longer stability, tunable transition frequency [11], and ease of implementation in a solid-state environment. Quantum dot single-photon sources are often coupled to photonic environments, such as micropillar cavities [12] or photonic crystal defects [11], to facilitate enhanced light-matter interaction and collection of emitted photons via cavity quantum electrodynamics (cavity QED), which also helps to minimize the coupling time to decoherence

processes. Cavity coupling can be used to exploit coherent phenomena characteristic of the strong-coupling regime of cavity QED, including coherent Rabi oscillations of excitonic populations—manifesting in strong-field phenomena such as Autler-Townes splitting of exciton energy levels [13,14], Mollow triplet emission spectra [15–18], or weak-coupling regimes such as the Purcell enhancement of spontaneous emission rates [19,20], allowing for increased collection efficiency of the emitted single photons [7,21].

Semiconductor cavity-QD systems are some of the most promising candidates for efficient, deterministic sources of indistinguishable single photons [11]. However, QD systems are not without their drawbacks. In particular, the solid-state nature of the QD leads to coupling of excitons with phonons, most notably, with longitudinal-acoustic (LA) phonons [22–28]. This coupling is often an intrinsic source of decoherence within QD photon sources and imposes fundamental limits on the efficacy of QDs as quantum light sources [29]. In particular, incoherent excitation schemes to invert exciton or biexciton populations typically involve pumping (e.g., with an above-resonant optical pulse) the QD to a higher energy level in the conduction band, and letting the QD relax to the exciton state through phonon-mediated transitions or other nonradiative processes [30–33]. This can introduce a timing “jitter”, or uncertainty, in the lifetime of the exciton state, reducing the indistinguishability of photons emitted [4,34,35]. Additionally, off-resonant excitation requires higher pump strengths, increasing phonon-induced dephasing rates [36]. As a result, incoherent off-resonant excitation schemes can produce photons with high efficiency (and robust to laser detunings) but poor indistinguishability, and are typically inferior to coherent pumping mechanisms for single-photon sources [36,37]. In contrast, this work studies a coherent pump-triggered excitation scheme via a modified version of stimulated Raman adiabatic passage (STIRAP) and cavity coupling. This scheme, initially proposed by Pathak and

*c.gustin@queensu.ca

Hughes [37] for a simple four-level atom system, uses the biexciton-exciton cascade—consisting of two linearly polarized excitons and a biexciton (two excitons) state—to coherently generate on-demand single photons of different polarization than the input pulse, allowing for spectral separation of pump from output light. While this approach shows promise, the original calculations were performed without any inclusion of electron-phonon coupling effects, which are known to play an important role in semiconductor QD-cavity systems [12,18,22,25,29,35,38,39].

In this work, we expand upon the simple atomlike Lindblad master equation (ME) approach [37] by introducing into the analysis an explicit model of electron-phonon interactions via a time-convolutionless polaron ME. Polaron MEs have been successfully used to explain a variety of phonon-related phenomena in QD systems, including Rabi frequency renormalization [40], phonon-modified QD emission spectra of exciton and biexciton states [17,41], off-resonant phonon-assisted population inversion [36], phonon-modified Purcell enhancement of spontaneous emission rates [38], and ultrafast polaritonic phonon dynamics in the strong coupling regime [42]. The polaronic ME approach allows one to numerically calculate the relevant figures of merit for a single-photon source, including the efficiency (quantified roughly via the expectation value of the number of photons emitted into the cavity), and the quantum indistinguishability, obtained from the two-time correlation functions of the cavity mode operators. The polaron transform is a unitary transform which shifts the analysis of exciton-phonon interactions to a quasiparticle “polaron” frame, where in the limit of zero laser or cavity coupling, the independent Boson model (IBM) [43] is recovered exactly, treating certain phonon coupling to a fermionic atom nonperturbatively. This allows for accurate and efficient computations to be made over a wide variety of temperatures, where other methods—such as a weak-coupling ME approach, which is perturbative in the exciton-phonon interaction and thus does not capture multiphonon processes [22]—fail. The polaron ME approach also has certain benefits over numerically exact path-integral approaches [44], such as providing more physical insight, as well as easier computation of quantum optics observables including two-time-correlation functions, which are necessary, e.g., for the calculation of the single-photon indistinguishability.

We show how this QD-cavity scheme produces single photons of high efficiency and indistinguishability, and we explore the role of temperature and phonon coupling in detail. We find that the STIRAP setup can allow for photons with simultaneously over 90% efficiency and indistinguishability to be generated even in the presence of LA phonon coupling using resonant pulse excitation, and with near unity efficiency and over 80% indistinguishability using off-resonant pulse excitation. The layout of the rest of our paper is as follows: In Sec. II we describe the theoretical formalism of the open system time-dependent quantum dynamics we use to model the QD-cavity single-photon source. In Sec. III, we solve the polaron ME for the system reduced density operator and two-time correlations of the cavity mode operators to calculate the expectation value of the number of photons emitted into the cavity per pulse excitation, and quantum indistinguishability of emitted photons. We also calculate the cavity-emitted spectrum

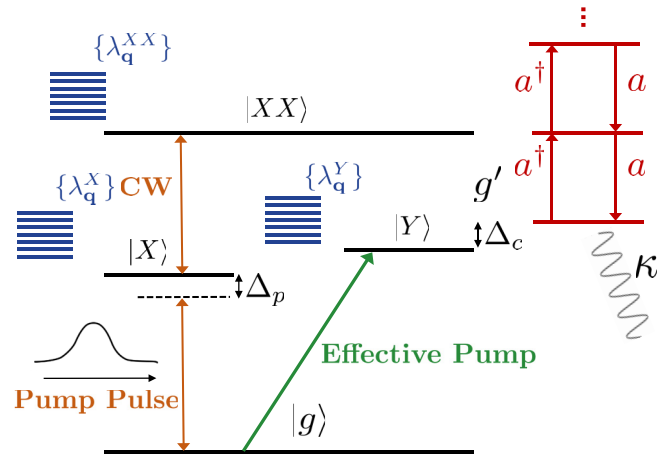


FIG. 1. Schematic of the STIRAP single-photon source excitation method in the biexciton cascade of a QD coupled to a cavity mode and phonon bath.

and explain its features in terms of the field dressing of the system eigenstates by the various field and cavity couplings in the presence of phonon coupling. Finally, we conclude in Sec. IV.

II. THEORETICAL MODEL

A. QD-cavity system Hamiltonian

We model the QD-cavity system with a four-level biexciton cascade scheme (see Fig. 1) coupled to a cavity mode with creation and destruction operators a^\dagger and a , respectively. Additionally, each excited state of the QD is coupled to a bath of phonon modes indexed by wave vector \mathbf{q} and with bosonic creation and destruction operators $b_{\mathbf{q}}^\dagger$ and $b_{\mathbf{q}}$. The ground to X -exciton (x -polarized) transition is coupled by a time-dependent optical pump pulse with Rabi frequency $\Omega_p(t)$, while the X -exciton to biexciton (XX) transition is coupled by a continuous-wave (cw) laser with Rabi frequency Ω_l . The cavity mode is chosen to couple the biexciton state to the Y exciton with coupling constant g . With appropriate choice of drive strengths, the system population is adiabatically transferred via the STIRAP process from the ground state to the Y exciton without significantly populating the X -exciton and biexciton states, in the process emitting a single photon into the cavity. The system then decays radiatively to the ground state, allowing the source to be triggered once again. Neglecting, for now, background decoherence of the zero-phonon line including cavity decay, spontaneous emission, and pure dephasing, the Hamiltonian for this system in a rotating frame (see the Appendix for the relevant unitary transformation) is

$$\begin{aligned}
 H = & \hbar \Delta_p |X\rangle \langle X| + \hbar(\Delta_p + \Delta_l - \Delta_c) |Y\rangle \langle Y| \\
 & + \hbar(\Omega_p(t) |X\rangle \langle g| + \Omega_l |XX\rangle \langle X| + g |XX\rangle \\
 & \times \langle Y| a + \text{H.c.}) + \hbar(\Delta_p + \Delta_l) |XX\rangle \langle XX| \\
 & + \sum_{\mathbf{q}} \hbar \omega_{\mathbf{q}} b_{\mathbf{q}}^\dagger b_{\mathbf{q}} + \sum_{S=\{X,Y,XX\}} |S\rangle \langle S| \sum_{\mathbf{q}} \hbar \lambda_{\mathbf{q}}^S (b_{\mathbf{q}}^\dagger + b_{\mathbf{q}}),
 \end{aligned} \tag{1}$$

with pump pulse detuning $\Delta_p \equiv \omega_X - \omega_p$, cw laser detuning $\Delta_l \equiv \omega_{XX} - \omega_l - \omega_X$, and cavity detuning $\Delta_c \equiv \omega_{XX} - \omega_Y - \omega_c$. For the multistage STIRAP process, the cw laser should be on resonance such that $\Delta_l = 0$, and $\Delta_p = \Delta_c$ to satisfy the multiphoton resonance condition [37,45]. Thus in the following analysis we set $\Delta_l = 0$ and define $\Delta \equiv \Delta_p = \Delta_c$. To ensure that none of the transitions between ground and exciton states simultaneously couple to exciton to biexciton transitions (and vice versa), the magnitude of the detuning Δ is assumed well below the biexciton binding energy (typically on the order of 1 meV) for the QD of interest such that $|\Delta| \ll |\omega_X - \frac{1}{2}\omega_{XX}|$. The LA phonon-exciton coupling is included via coupling constants $\{\lambda_q^S\}$ for $S = \{X, Y, XX\}$, which are assumed to be real and correspond to an ideal quantum confined QD such that $\lambda_q \equiv \lambda_q^X = \lambda_q^Y = \frac{1}{2}\lambda_q^{XX}$ [46].

B. Polaron master equation

To analyze the dynamics of the STIRAP single-photon source, we develop an open-system time-local ME approach to determine the reduced system density matrix and calculate relevant quantities. To incorporate effects of the phonon bath, we first apply a polaron transform of the form $H' = e^S H e^{-S}$ to approximately (exactly in the limit of no field couplings) diagonalize the Hamiltonian in the polaron frame, where $S = (2|XX\rangle\langle XX| + |X\rangle\langle X| + |Y\rangle\langle Y|) \sum_q \frac{\lambda_q}{\omega_q} (b_q^\dagger + b_q)$. Separating the polaron-transformed Hamiltonian H' into system, bath, and interaction parts such that $H' = H'_S + H'_B + H'_I$, we have

$$\begin{aligned} H'_S &= (\Delta - \delta_P) |X\rangle\langle X| \\ &+ (\Delta - 2\delta_P) |XX\rangle\langle XX| - \delta_P |Y\rangle\langle Y| \\ &+ (\Omega'_p(t) |X\rangle\langle g| + \Omega'_l |XX\rangle\langle X| + g' |XX\rangle \\ &\times \langle Y| a + \text{H.c.}), \end{aligned} \quad (2)$$

where $\delta_P = \sum_q \frac{\lambda_q^2}{\omega_q}$ is a Lamb shift in the exciton energies due to phonon bath renormalization. We assume that this polaron shift is absorbed into the original definitions of Δ_p , Δ_c , and Δ_l such that it can be neglected henceforth. The drive strengths and cavity coupling $\Omega'_p(t) = \langle B \rangle \Omega_p(t)$, $\Omega'_l = \langle B \rangle \Omega_l$, and $g' = \langle B \rangle g$ are coherently reduced by the presence of the phonon bath, where $\langle B \rangle = \langle B_+ \rangle = \langle B_- \rangle = \exp[-\frac{1}{2} \sum_q \frac{\lambda_q^2}{\omega_q^2} \coth(\frac{\hbar\omega_q}{2k_B T})]$ is the thermal average of the coherent displacement operators $B_\pm = \exp[\pm \sum_q \frac{\lambda_q}{\omega_q} (b_q^\dagger - b_q)]$. The free Hamiltonian of the phonon bath is given by $H'_B = \sum_q \hbar\omega_q b_q^\dagger b_q$, and the interaction Hamiltonian is $H'_I = X_g \zeta_g + X_u \zeta_u$, with drive operators $X_g = \hbar\Omega_p(t) |X\rangle\langle g| + \hbar\Omega_l |XX\rangle\langle X| + \hbar g |XX\rangle\langle Y| a + \text{H.c.}$, and $X_u = i(\hbar\Omega_p(t) |X\rangle\langle g| + \hbar\Omega_l |XX\rangle\langle X| + \hbar g |XX\rangle\langle Y| a) + \text{H.c.}$, and phonon fluctuation operators $\zeta_g = \frac{1}{2}(B_+ + B_- - 2\langle B \rangle)$ and $\zeta_u = \frac{1}{2i}(B_+ - B_-)$.

We assume a continuous spectrum of phonon modes such that $J(\omega) = \sum_q \lambda_q^2 \delta(\omega - \omega_q) \rightarrow J(\omega) = \alpha \omega^3 \exp[-\frac{\omega^2}{2\omega_b^2}]$, which is the form of the phonon spectral function $J(\omega)$ appropriate for describing a deformation potential induced by LA phonons—the main source of phonon-related decoherence in QD single-photon sources [22–24]; α is the exciton-phonon

coupling strength, and ω_b is the phonon cut-off frequency. Following Refs. [18,41], we derive a time-local second-order Born-Markov ME in the polaron frame

$$\begin{aligned} \frac{d}{dt} \rho(t) &= -\frac{i}{\hbar} [H'_S, \rho(t)] - \frac{1}{\hbar^2} \int_0^\infty d\tau \sum_{m=\{g,u\}} \{G_m(\tau) \\ &\times [X_m(t), X_m(t, \tau) \rho(t)] + \text{H.c.}\} + \sum_\mu \mathcal{L}[O_\mu] \rho(t), \end{aligned} \quad (3)$$

where $G_g(\tau) = \langle B \rangle^2 \{\cosh[\phi(\tau)] - 1\}$ and $G_u(\tau) = \langle B \rangle^2 \sinh[\phi(\tau)]$ are the polaron Green's functions, and $X_m(t, \tau) \approx e^{-iH'_S(t)\tau/\hbar} X_m(t) e^{iH'_S(t)\tau/\hbar}$. In the continuum limit, we have the following IBM phase function:

$$\phi(\tau) = \int_0^\infty d\omega \frac{J(\omega)}{\omega^2} \left[\coth\left(\frac{\hbar\omega}{2k_B T}\right) \cos(\omega\tau) - i \sin(\omega\tau) \right], \quad (4)$$

with $\langle B \rangle = e^{-\phi(0)/2}$, and this function includes multiple phonon absorption and emission transitions. Note that the polaron transform approach is rigorously valid in the regime where, for a given Rabi frequency, $(\frac{\Omega}{\omega_b})^2 (1 - \langle B \rangle)^4 \ll 1$, which is the case for the parameters used here [40]. Additionally, to phenomenologically include decohering processes beyond LA phonon-exciton coupling [18], we include Lindblad terms (for collapse operator O : $\mathcal{L}[O]\rho \equiv O\rho O^\dagger - \frac{1}{2}\{O^\dagger O, \rho\}$), corresponding to collapse operators $\sqrt{\gamma_{XX}} |X\rangle\langle XX|$, $\sqrt{\gamma_{XX}} |Y\rangle\langle XX|$, $\sqrt{\gamma_X} |g\rangle\langle X|$, $\sqrt{\gamma_X} |g\rangle\langle Y|$ (i.e., $\gamma_X = \gamma_Y$) corresponding to spontaneous emission, as well as $\sqrt{2\gamma'} |XX\rangle\langle XX|$, $\sqrt{\gamma'} |X\rangle\langle X|$, and $\sqrt{\gamma'} |Y\rangle\langle Y|$ corresponding to pure dephasing. We furthermore introduce cavity photon leakage via collapse operator $\sqrt{\kappa} a$, appropriate for good cavities [38]. Initially the QD (assumed to be neutrally charged) is taken to be in the ground state and the cavity mode in the vacuum state.

To calculate the key figures of merit for this single-photon source in the presence of phonons, the ME of Eq. (3) is first solved numerically. We then quantify the efficiency of the source with the emitted cavity photon number, $N_e \equiv \lim_{t \rightarrow \infty} P_e(t)$, with $P_e(t) = \int_0^t \kappa \langle a^\dagger a \rangle(t') dt'$. Following previous works [34,37,47], we can quantify the indistinguishability of the single photons by considering a Hong-Ou-Mandel interferometry setup, where two photons consecutively emitted from the single-photon source are directed at a beam splitter. The indistinguishability, \mathcal{I} , of the photons determines the degree to which two-photon interference is observed, and can be expressed in terms of the cavity mode correlation functions:

$$\mathcal{I} \equiv \lim_{T \rightarrow \infty} \frac{1}{2} \left[1 - \frac{\int_0^T dt \int_0^{T-t} d\tau [g^{(2)}(t, \tau) - |g^{(1)}(t, \tau)|^2]}{\int_0^T dt \int_0^{T-t} d\tau \langle a^\dagger a \rangle(t) \langle a^\dagger a \rangle(t + \tau)} \right], \quad (5)$$

where $g^{(1)}(t, \tau) = \langle a^\dagger(t) a(t + \tau) \rangle$ and $g^{(2)}(t, \tau) = \langle a^\dagger(t) a^\dagger(t + \tau) a(t + \tau) a(t) \rangle$ are the quantum degrees of first- and second-order coherence, respectively, which are calculated from the ME solution via the quantum regression theorem [48].

III. RESULTS

Throughout this work, we use parameters $\gamma_{XX} = \gamma_X = 0.5 \text{ ns}^{-1}$ ($0.33 \text{ } \mu\text{eV}$) and $\kappa = 25 \text{ ns}^{-1}$ ($16.5 \text{ } \mu\text{eV}$). The background pure dephasing rate (e.g., due to charge, spin noise), except where chosen as a parameter to vary, is $\gamma' = 1 \text{ ns}^{-1}$ ($0.66 \text{ } \mu\text{eV}$). The phonon parameters are chosen to be $\alpha = 0.03 \text{ ps}^2$ and $\omega_b = 0.9 \text{ meV}$, similar to those found from the experimental results by Quilter *et al.* [32]. The phonon coupling strength α can vary from dot to dot, and so we also show in Fig. 2(a) the phonon bath mean displacement for a value of $\alpha = 0.06 \text{ ps}^2$, as found in the experimental results by Weiler *et al.* [49]. To optimize the STIRAP process [50], we take the pump pulse profile to be sawtooth (see Fig. 3) with max pulse strength $\Omega'_p = 2.5g'$ and pulse width $g'\tau_p = 3\pi$ throughout, except in Fig. 8 where the pulse width is varied. Note that we have numerically confirmed that the sawtooth pulse shape can be substituted – for example, with a Gaussian – with negligible effects on the system figures-of-merit, provided that the pulse area $\int_0^\infty \Omega(t)dt$ remains the same. The CW laser strength is fixed at $\Omega'_l = 5g'$. Except in Fig. 4, where we show the effects of the coherent renormalization of coupling parameters by the phonon bath, we take $g' = 50 \text{ ns}^{-1}$ ($32.9 \text{ } \mu\text{eV}$) to be a constant throughout, noting that the zero-temperature cavity coupling, Rabi frequencies, and pulse width must be modified by a factor of $\langle B \rangle$ to accurately compare the incoherent effects of the phonon bath, which are of interest, as they limit the efficiency and indistinguishability of the single-photon source. The renormalization effect is quite small at low temperatures, and a mean bath displacement of $\langle B \rangle = 0.96$ at $T = 5 \text{ K}$ only affects the emitted photon number by less than 0.005 with

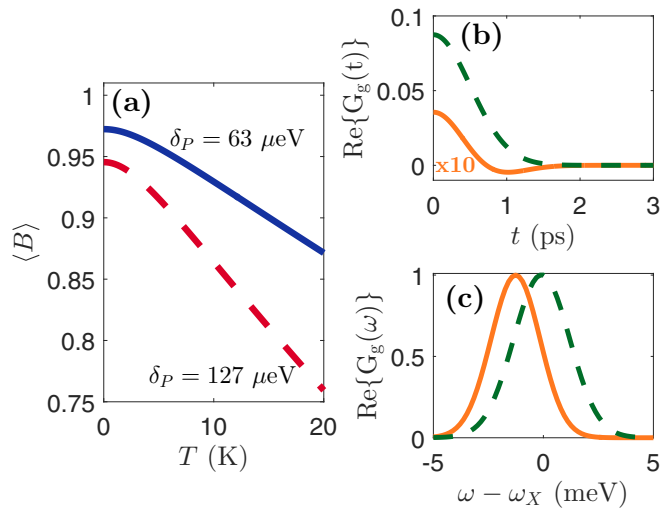


FIG. 2. (a) Phonon bath mean displacement $\langle B \rangle$ (drive strength and cavity coupling renormalization factor) as a function of temperature for $\alpha = 0.03 \text{ ps}^2$ (blue, solid) and $\alpha = 0.06 \text{ ps}^2$ (red, dotted), as well as the associated polaron shifts $\delta_p = \int_0^\infty d\omega J(\omega)/\omega$. (b) Real part of one of the polaron Green's functions $G_g(t)$, giving the time evolution of the bath correlation function (for an exciton state) with $\alpha = 0.03 \text{ ps}^2$ for $T = 5 \text{ K}$ (dotted green line) and $T = 40 \text{ K}$ (solid orange line). (c) Real part of $G_g(\omega)$ in the frequency domain, showing a low-temperature asymmetry of phonon bath correlations.

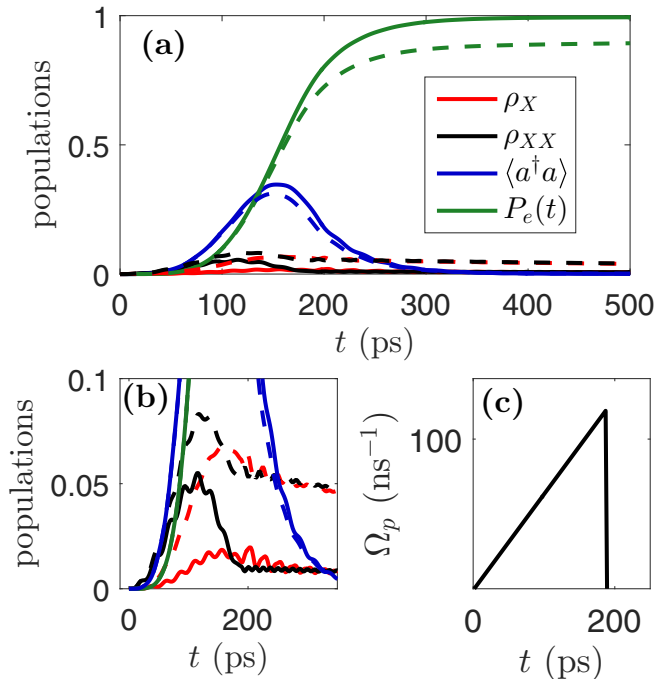


FIG. 3. (a) Populations of X exciton (ρ_X ; red), biexciton (ρ_{XX} ; black), cavity ($\langle a^\dagger a \rangle$; blue), as well as the emitted photon number [$P_e(t)$; green] with (dashed lines) and without (solid lines) the exciton-phonon interaction. (b) Inset of plot in (a). (c) Pump pulse time profile, with max pulse strength $2.5g'$ and pulse width $3\pi/g'$.

these excitation parameters. Unless otherwise specified, all results with phonons are at the bath temperature of $T = 5 \text{ K}$. Simulating results here “without phonons” means that the incoherent exciton-phonon scattering terms in Eq. (3) are set to zero and the cavity and field couplings are not renormalized by the factor of $\langle B \rangle$.

Figure 3 displays the populations of various QD states and the cavity mode over time, showing the influence of incoherent

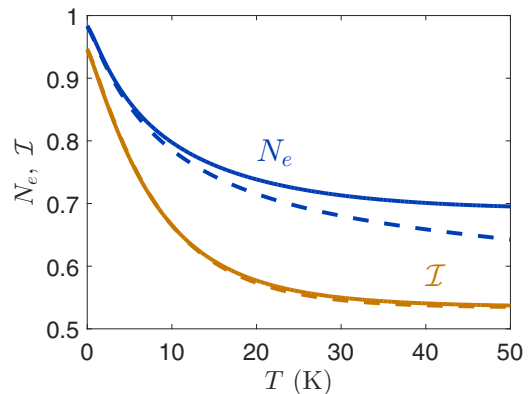


FIG. 4. Effect of phonon renormalization of excitation parameters. Shown is the emitted photon number and indistinguishability for constant (temperature-independent) bare coupling parameters g, Ω_l, Ω_p (dashed lines) and constant effective coupling parameters g', Ω_l', Ω_p' (solid lines). We use a temperature-dependent dephasing rate $\gamma'(T) = \gamma'_0 + (2.127 \text{ ns}^{-1}/\text{K})T$ with $\gamma'_0 = 1 \text{ ns}^{-1}$, as discussed in the main text.

exciton-phonon scattering. Without phonons, these simulation parameters give an emitted photon number $N_e = 1.00$ and indistinguishability $\mathcal{I} = 0.96$, and with phonons, $N_e = 0.93$ and $\mathcal{I} = 0.90$. The presence of phonons indeed increases the degree to which the intermediate states (X exciton and biexciton) in the STIRAP process are populated, decreasing the efficiency of the adiabatic population transfer. This can be attributed to additional phonon-induced dephasing captured in the polaron ME, reducing the coherence of the transfer process, as well as transitions between states mediated by phonon absorption and emission. Note that the finite lifetime of the Y -exciton state means that there is a small probability of the exciton decaying to the QD ground state and being reexcited during the same pump pulse, emitting two photons into the cavity. This limits the indistinguishability of the emitted photons and thus overly long pulse widths should be avoided. This also means that longer excited-state lifetimes (specifically, the Y -exciton lifetime [37]) improve the indistinguishability of the emitted photons, suggesting that this setup could benefit from the reduction of the density of optical states away from cavity resonance, which, e.g., can be achieved with a photonic crystal cavity [38].

The spectral width (decay rate) κ of the cavity is important to the performance of this STIRAP single-photon source. For example, if it is too small, the cavity mode and biexciton state will sustain Rabi oscillations. This is disadvantageous because it increases the population of the biexciton state (even if only transiently), which exposes the system to additional decoherence including spontaneous emission into noncavity modes, phonon coupling, and other dephasing processes. If it is too large, the biexciton state will decouple from the Y exciton before the population transfer is complete, as $|XX\rangle$ does not coherently couple to the state $|Y\rangle \otimes |0\rangle$ (where $|0\rangle$ is the cavity mode vacuum state). We plot the cavity populations as well as the associated figures of merit (N_e , \mathcal{I}) for various values of κ in Fig. 5 to further illustrate this. For the smallest cavity width, the efficiency drops without much change in the indistinguishability. This is because—as has been demonstrated in recent works—the cavity acts as a spectral filter, filtering out photons emitted into the phonon sideband, decreasing efficiency while improving indistinguishability [29,51]. Note that while the cavity parameters place the

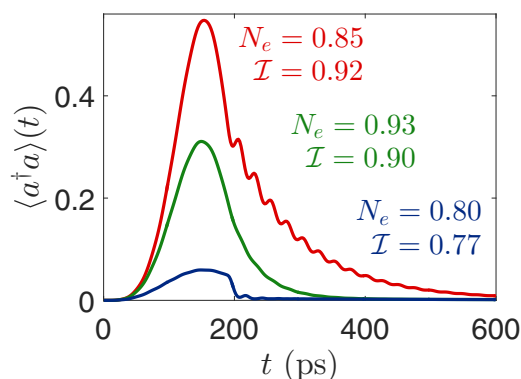


FIG. 5. Cavity population as a function of time for a resonant ($\Delta = 0$) pulse with $\kappa = g'/5$ (red), $\kappa = g'/2$ (green), and $\kappa = 2g'$ (blue), along with the emitted photon number and indistinguishability for each case (phonons included for all cases).

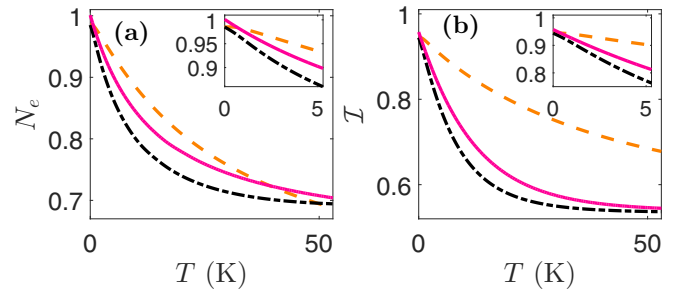


FIG. 6. (a) Number of photons emitted into cavity N_e and (b) indistinguishability \mathcal{I} as a function of temperature with phonons and constant dephasing $\gamma'_0 = 1$ ns $^{-1}$ (dashed orange line), with a temperature-dependent dephasing $\gamma'(T) = \gamma'_0 + (2.127$ ns $^{-1}$ /K)T and no phonons (solid magenta line), and with both phonons and temperature-variable dephasing (black dash-dotted line).

cavity-QD coupling in the intermediate-to-strong-coupling regime ($4g > \kappa$), typical features of the strong-coupling regime (pronounced Rabi oscillations) are not as prominent, as the cavity mode should adiabatically follow the pump pulse in ideal performance.

In addition to increased exciton-phonon coupling strengths at higher temperatures (which are intrinsic to the QD), other processes (e.g., charge noise in QDs), including phonon effects beyond the IBM, have dephasing rates which are often dependent on temperature [52]. In Fig. 6 we study the device performance over a wide range of potential operating temperatures by comparing the relative effects of phonon coupling versus temperature-dependent background pure dephasing rates. Following the experimental results in Ref. [53], we employ an empirical linear pure dephasing correlation $\gamma'(T) = \gamma'_0 + (2.127$ ns $^{-1}$ /K)T with $\gamma'_0 = 1$ ns $^{-1}$ and study the special case of resonant excitation ($\Delta = 0$) with pulse parameters as used elsewhere in this section. Recent work has shown that at temperatures above ~ 10 K, acoustic phonons may induce virtual transitions to higher-lying QD excited states, which, when analyzed using an effective two-level system approach, manifests as a highly non-linear pure dephasing as a function of temperature [54]. We thus emphasize that our results quoted as “with phonons” really refer to the linear exciton-phonon interaction, as found in the IBM and dominant at low temperatures. Fig. 6 suggests that at low temperatures (4 K), intrinsic linear phonon coupling has a less detrimental effect on device figures of merit than that of increased pure dephasing rates, which are not fundamental limitations and indeed have been shown to be significantly suppressed in recent experiments [7,55].

Next, in Fig. 7, we study the effects of varying the pump pulse and cavity detuning Δ . Very high efficiencies ($\sim 99\%$) are achieved at detunings of $\Delta = \pm\Omega_l = \pm 164.5$ μ eV (250 ns $^{-1}$), which can be attributed to the Autler-Townes splitting of the biexciton state by $\pm\Omega_l$ due to the cw laser drive. Positive detunings produce photons of higher indistinguishability, as in this case, the pump pulse and cavity detunings are below resonance with respect to the exciton state transitions, practically avoiding phonon-emission-mediated transitions. Since the number of phonons present in a thermal bath is small at low temperatures, phonon-absorption processes are less

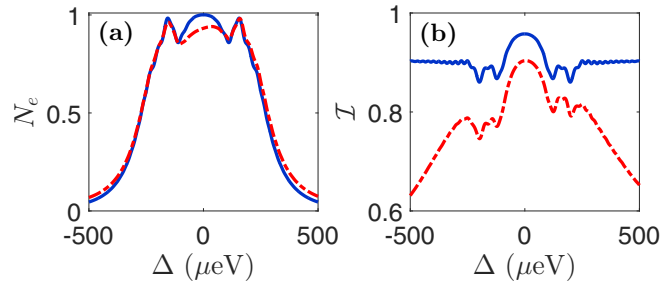


FIG. 7. (a) Emitted cavity photon number and (b) indistinguishability without phonons (solid blue line) and with phonons (dash-dotted red line) as a function of pulse and cavity detuning $\Delta = \Delta_c = \Delta_p$.

influential. One potential advantage of off-resonant excitation is that, for positive values of Δ , it ensures that the cavity mode in which photons are emitted into is not only of an orthogonal polarization to the pump and cw light, but also a different frequency, potentially aiding in photon collection and filtering. Even on resonance, the presence of fine-structure anisotropic exchange splitting between X - and Y -polarized exciton states renders the cavity mode a different frequency than the applied fields, but the degree of the splitting is small (~ 10 – $100 \mu\text{eV}$) and varies from dot to dot [11]. To further study this off-resonant excitation scheme, we take $\Delta = 158 \mu\text{eV}$ and show the effect of varying the pulse width in Fig. 8, along with the corresponding result for resonant excitation ($\Delta = 0$). Note that for this detuning, the system evolves less adiabatically, directly using the lower energy state of the Autler-Townes doublet formed in the presence of the cw drive as an intermediate state.

It is also interesting to probe the field-induced state dressing that occurs through the cavity-emitted spectrum, which is easily accessed experimentally [15,16,56–58]. In Fig. 9, we plot the cavity-emitted spectrum with and without phonons for resonant excitation. The emission spectrum from pulsed excitation in the laboratory frame can be found from the Fourier transform of the time-averaged cavity mode first-order correlation function [59]:

$$S_c(\omega) \equiv \text{Re} \left[\int_0^\infty d\tau e^{-i(\omega - \omega_c)\tau} \int_0^\infty dt \langle a^\dagger(t + \tau)a(t) \rangle \right]. \quad (6)$$

The spectrum on resonance resembles that of the well-known Mollow triplet with a cw drive [60], but has a somewhat

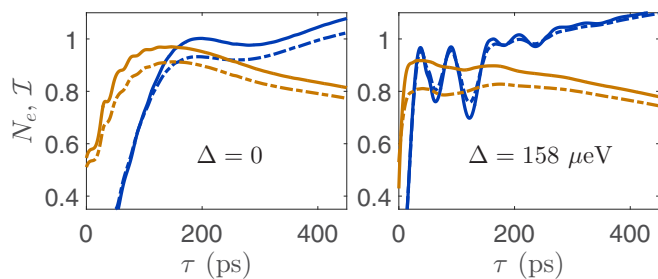


FIG. 8. Emitted cavity photon number (blue) and indistinguishability (brown) for on-resonant (left) and off-resonant (right) excitation with phonons (dashed lines) and without (solid lines).

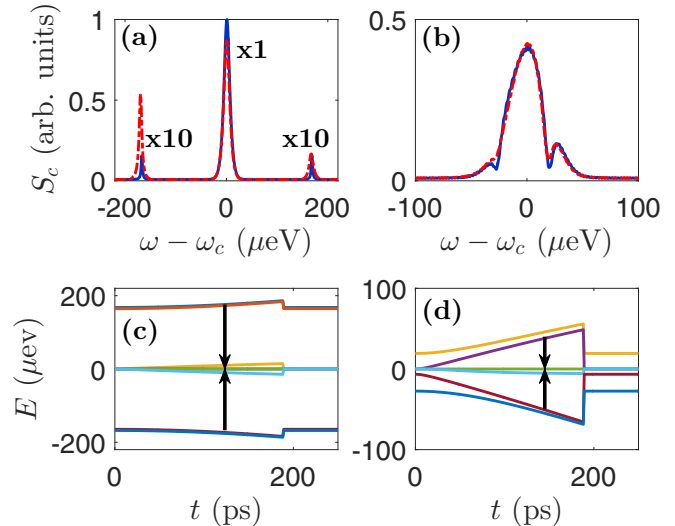


FIG. 9. Top: Cavity-emitted spectra $S_c(\omega)$ for (a) an on-resonance pulse with $\Delta = 0 \mu\text{eV}$ and (b) an off-resonance pulse with $\Delta = 158 \mu\text{eV}$, with phonons (dash-dotted red line) and without (solid blue line). Bottom: Quasieigenenergies of system Hamiltonian in rotating frame (see Appendix) as a function of time for (c) $\Delta = 0 \mu\text{eV}$ and (d) $\Delta = 158 \mu\text{eV}$, truncated to a one-photon (two-dimensional) Fock space, showing nonadiabatic transitions that create side peaks in the cavity-emitted spectrum.

different physical origin. The side peaks in the spectrum arise from biexciton to Y -exciton transitions, where the biexciton state is split by $\pm\Omega_l$ due to the presence of the cw drive. For efficient on-resonance STIRAP population transfer, the intermediate (biexciton state) is never significantly populated due to destructive interference in the probability amplitude of transitioning to either of the two energy levels split from the cw laser dressing the X -exciton to biexciton transition [61], and the side peaks in the cavity-emitted spectrum are thus very small. As the (phonon-induced) dephasing is increased, the intermediate state is partly populated, leading to off-resonant side peaks in the spectrum which are enhanced by phonon absorption and emission processes, asymmetrically favoring phonon emission at low temperatures. Since a lack of sidebands in the emission spectrum (barring any postselection) is a necessary condition (although not sufficient—two-photon emission events must also be suppressed) for indistinguishable photons, this interruption of the STIRAP process by the intermediate eigenstate population can allow for high emitted photon number, but with a cost of lower indistinguishability [29]. The somewhat odd shape of the off-resonant spectrum is partially due to simultaneous field dressing of different transitions, causing ac Stark shifts which lead to a complicated eigenstructure [41]. The main side peaks can be attributed to additional splitting of the lower rung of the Autler-Townes doublet arising from the cw drive by the cavity mode. Also shown in Fig. 9 are the system time-dependent quasieigenenergies corresponding to each respective spectra. In the rotating frame, transitions between different system eigenstates (shown as black arrows) correspond to side peaks in the cavity-emitted spectrum (the exact location of which depends on the details of the relevant eigenstate populations over time). The eigenvalues

of the system Hamiltonian [Eq. (2)] in the rotating frame also can be used to study the mechanism behind the single-photon emission. In ideal STIRAP, the system remains in a zero-eigenvalue state during the entire population transfer process [61], and side peaks in the cavity spectrum are very small. For the off-resonant case [Fig. 9(b)], we see much larger side peaks relative to the main peak both with and without phonons, indicating high population of the undesired nonzero eigenvalue dressed states, suggesting that additional phonon-induced dephasing is the dominant decoherence mechanism for this detuning.

Finally, we note that the STIRAP excitation scheme in this work can be modified by eliminating the cw laser coupling the X -exciton to biexciton transition and using the pump pulse to couple the ground state to biexciton transition directly via two-photon resonance. This makes the pump process simpler, but is less effective, requiring longer pulse widths to compensate for the lack of strong Autler-Townes splitting by the cw drive, which increases the influence of dephasing on the system [61] and yields indistinguishabilities not higher than 80% for parameters (excluding the pulse strength and width) similar to those used in the rest of this section.

IV. CONCLUSIONS

In summary, we have analyzed a coherently triggered QD single-photon source utilizing STIRAP with a polaron ME approach which accurately incorporates effects of intrinsic electron-phonon scattering. Our results, using realistic experimental parameters, show that simultaneous achievement of over 90% efficiency and indistinguishability, or near-unity efficiency and over 80% indistinguishability using this setup should be possible, even in the presence of electron-phonon scattering.

While this source is advantageous in that it combines high indistinguishabilities and efficiencies with easily filtered emitted photons, for near-unity indistinguishabilities (which are typically required in proposals for all-optical quantum computing [62]), recent experiments using resonant pulsed excitation [7] and rapid adiabatic passage [63] to invert the exciton state coupled to a cavity have demonstrated higher success than our results would suggest for the STIRAP scheme studied in this work; however, the overall fidelity of these single-photon sources is limited by the fact that simultaneously

very high efficiency (brightness) and indistinguishability has yet to be achieved, partially due to the difficulty in effectively filtering and collecting photons under these coherent excitation methods, as the pump field is often resonant with the emitted single photons, requiring polarization discrimination (thus reducing the efficiency and “on-demand” nature of the single photon gun). In contrast, by emitting single photons into a strongly coupled cavity mode of an orthogonal polarization (and potentially different resonant frequency) to the applied fields, the STIRAP setup here allows for high emission efficiencies and trivially filtered laser light.

ACKNOWLEDGMENTS

This work was supported by the Natural Sciences and Engineering Research Council of Canada (NSERC) and Queen’s University. We thank R. Manson and K. Roy-Choudhury for useful discussions.

APPENDIX: ROTATING FRAME TRANSFORMATION

Starting from the Hamiltonian:

$$\begin{aligned}
 H = & \sum_{S=\{X,Y,XX\}} \hbar\omega_S |S\rangle \langle S| + \hbar\omega_c a^\dagger a \\
 & + 2\hbar[\Omega_l \cos(\omega_l t) |XX\rangle \langle X| \\
 & + \Omega_p(t) \cos(\omega_p t) |X\rangle \langle g| + g \cos(\omega_c t) |XX\rangle \\
 & \times \langle Y| a + \text{H.c.}] + \sum_{\mathbf{q}} \hbar\omega_{\mathbf{q}} b_{\mathbf{q}}^\dagger b_{\mathbf{q}} \\
 & + \sum_{S=\{X,Y,XX\}} |S\rangle \langle S| \sum_{\mathbf{q}} \hbar\lambda_{\mathbf{q}}^S (b_{\mathbf{q}}^\dagger + b_{\mathbf{q}}), \quad (\text{A1})
 \end{aligned}$$

we move into the interaction picture with the Hamiltonian $\tilde{H}_I = e^{iH_0 t/\hbar} H_I e^{-iH_0 t/\hbar}$ by defining $H = H_0 + H_I$, with

$$\begin{aligned}
 H_0 = & \hbar\omega_p |X\rangle \langle X| + \hbar(\omega_p + \omega_l - \omega_c) |Y\rangle \langle Y| \\
 & + \hbar(\omega_p + \omega_l) |XX\rangle \langle XX| + \hbar\omega_c a^\dagger a. \quad (\text{A2})
 \end{aligned}$$

Expanding the cosines in Eq. (A1) as complex exponentials and dropping terms proportional to $\exp(\pm i2\omega t)$ (rotating-wave approximation), one arrives at the rotating frame (interaction picture) Hamiltonian used in Eq. (1).

-
- [1] E. Knill, R. Lafamme, and G. J. Milburn, *Nature (London)* **409**, 46 (2001).
- [2] P. A. Hiskett, D. Rosenberg, C. G. Peterson, R. J. Hughes, S. Nam, A. E. Lita, A. J. Miller, and J. E. Nordholt, *New J. Phys.* **8**, 193 (2006).
- [3] P. Kok, W. J. Munro, K. Nemoto, T. C. Ralph, J. P. Dowling, and G. J. Milburn, *Rev. Mod. Phys.* **79**, 135 (2007).
- [4] A. Nazir and S. D. Barrett, *Phys. Rev. A* **79**, 011804(R) (2009).
- [5] J. Bylander, I. Robert-Philip, and I. Abram, *Eur. Phys. J. D* **22**, 295 (2003).
- [6] M. D. Reed, B. M. Maune, R. W. Andrews, M. G. Borselli, K. Eng, M. P. Jura, A. A. Kiselev, T. D. Ladd, S. T. Merkel, I. Milosavljevic, E. J. Pritchett, M. T. Rakher, R. S. Ross, A. E. Schmitz, A. Smith, J. A. Wright, M. F. Gyure, and A. T. Hunter, *Phys. Rev. Lett.* **116**, 110402 (2016).
- [7] N. Somaschi *et al.*, *Nat. Photon.* **10**, 340 (2016).
- [8] A. V. Kuhlmann, J. Houel, A. Ludwig, L. Greuter, D. Reuter, A. D. Wieck, M. Poggio, and R. J. Warburton, *Nat. Phys.* **9**, 570 (2013).
- [9] S. Buckley, K. Rivoire, and J. Vučković, *Rep. Prog. Phys.* **75**, 126503 (2012).
- [10] D. C. Unitt, A. J. Bennett, P. Atkinson, K. Cooper, P. See, D. Gevaux, M. B. Ward, R. M. Stevenson, D. A. Ritchie, and A. J. Shields, *J. Opt. B: Quantum Semiclass. Opt.* **7**, S129 (2005).
- [11] P. Lodahl, S. Mahmoodian, and S. Stobbe, *Rev. Mod. Phys.* **87**, 347 (2015).

- [12] S. M. Ulrich, S. Ates, S. Reitzenstein, A. Löffler, A. Forchel, and P. Michler, *Phys. Rev. Lett.* **106**, 247402 (2011).
- [13] X. Xu, B. Sun, P. R. Berman, D. G. Steel, A. S. Bracker, D. Gammon, and L. J. Sham, *Science* **317**, 929 (2007).
- [14] J. P. Reithmaier, G. Şek, A. Löffler, C. Hofmann, S. Kuhn, S. Reitzenstein, L. V. Keldysh, V. D. Kulakovskii, T. L. Reinecke, and A. Forchel, *Nature (London)* **432**, 197 (2004).
- [15] E. B. Flagg, A. Muller, J. W. Robertson, S. Founta, D. G. Deppe, M. Xiao, W. Ma, G. J. Salamo, and C. K. Shih, *Nat. Phys.* **5**, 203 (2009).
- [16] A. Ulhaq, S. Weiler, C. Roy, S. M. Ulrich, M. Jetter, S. Hughes, and P. Michler, *Opt. Express* **21**, 4382 (2013).
- [17] C. Roy and S. Hughes, *Phys. Rev. Lett.* **106**, 247403 (2011).
- [18] C. Roy and S. Hughes, *Phys. Rev. B* **85**, 115309 (2012).
- [19] J. M. Gérard, B. Sermage, B. Gayral, B. Legrand, E. Costard, and V. Thierry-Mieg, *Phys. Rev. Lett.* **81**, 1110 (1998).
- [20] L. Balet, M. Francardi, A. Geradino, N. Chauvin, B. Alloing, C. Zinoni, C. Monat, L. H. Li, N. L. Thomas, R. Houdré, and A. Fiore, *Appl. Phys. Lett.* **91**, 123115 (2007).
- [21] X. Ding, Y. He, Z.-C. Duan, N. Gregersen, M.-C. Chen, S. Unsleber, S. Maier, C. Schneider, M. Kamp, S. Höfling, C.-Y. Lu, and J.-W. Pan, *Phys. Rev. Lett.* **116**, 020401 (2016).
- [22] A. Nazir and D. P. S. McCutcheon, *J. Phys.: Condens. Matter* **28**, 103002 (2016).
- [23] A. J. Ramsay, A. V. Gopal, E. M. Gauger, A. Nazir, B. W. Lovett, A. M. Fox, and M. S. Skolnick, *Phys. Rev. Lett.* **104**, 017402 (2010).
- [24] A. J. Ramsay, T. M. Godden, S. J. Boyle, E. M. Gauger, A. Nazir, B. W. Lovett, A. M. Fox, and M. S. Skolnick, *Phys. Rev. Lett.* **105**, 177402 (2010).
- [25] B. Krummheuer, V. M. Axt, and T. Kuhn, *Phys. Rev. B* **65**, 195313 (2002).
- [26] A. Vagov, V. M. Axt, and T. Kuhn, *Phys. Rev. B* **66**, 165312 (2002).
- [27] J. Förstner, C. Weber, J. Danckwerts, and A. Knorr, *Phys. Rev. Lett.* **91**, 127401 (2003).
- [28] L. Besombes, K. Kheng, L. Marsal, and H. Mariette, *Phys. Rev. B* **63**, 155307 (2001).
- [29] J. Iles-Smith, D. P. S. McCutcheon, A. Nazir, and J. Mørk, *Nat. Photonics* **11**, 521 (2017).
- [30] M. Glässl, A. M. Barth, and V. M. Axt, *Phys. Rev. Lett.* **110**, 147401 (2013).
- [31] S. Bounouar, M. Müller, A. M. Barth, M. Glässl, V. M. Axt, and P. Michler, *Phys. Rev. B* **91**, 161302(R) (2015).
- [32] J. H. Quilter, A. J. Brash, F. Liu, M. Glässl, A. M. Barth, V. M. Axt, A. J. Ramsay, M. S. Skolnick, and A. M. Fox, *Phys. Rev. Lett.* **114**, 137401 (2015).
- [33] Y. Toda, O. Moriwaki, M. Nishioka, and Y. Arakawa, *Phys. Rev. Lett.* **82**, 4114 (1999).
- [34] A. Kiraz, M. Atatüre, and A. Imamoglu, *Phys. Rev. A* **69**, 032305 (2004).
- [35] P. Kaer, N. Gregersen, and J. Mørk, *New J. Phys.* **15**, 035027 (2013).
- [36] R. Manson, K. Roy-Choudhury, and S. Hughes, *Phys. Rev. B* **93**, 155423 (2016).
- [37] P. K. Pathak and S. Hughes, *Phys. Rev. B* **82**, 045308 (2010).
- [38] K. Roy-Choudhury and S. Hughes, *Optica* **2**, 434 (2015).
- [39] U. Hohenester, *Phys. Rev. B* **81**, 155303 (2010).
- [40] D. P. S. McCutcheon and A. Nazir, *New J. Phys.* **12**, 113042 (2010).
- [41] F. Hargart, M. Müller, K. Roy-Choudhury, S. L. Portalupi, C. Schneider, S. Höfling, M. Kamp, S. Hughes, and P. Michler, *Phys. Rev. B* **93**, 115308 (2016).
- [42] K. Müller, K. A. Fischer, A. Rundquist, C. Dory, K. G. Lagoudakis, T. Sarmiento, Y. A. Kelaita, V. Borish, and J. Vučković, *Phys. Rev. X* **5**, 031006 (2015).
- [43] G. D. Mahan, *Many-Particle Physics*, 2nd ed. (Plenum, New York, 1990).
- [44] A. Vagov, M. D. Croitoru, M. Glässl, V. M. Axt, and T. Kuhn, *Phys. Rev. B* **83**, 094303 (2011).
- [45] N. V. Vitanov and S. Stenholm, *Phys. Rev. A* **60**, 3820 (1999).
- [46] U. Hohenester, G. Pfanner, and M. Seliger, *Phys. Rev. Lett.* **99**, 047402 (2007).
- [47] A. Kiraz, M. Atatüre, and A. Imamoglu, *Phys. Rev. A* **70**, 059904(E) (2004).
- [48] H. J. Carmichael, *Statistical Methods in Quantum Optics I: Master Equations and Fokker-Planck Equations* (Springer-Verlag, Berlin, 1999).
- [49] S. Weiler, A. Ulhaq, S. M. Ulrich, D. Richter, M. Jetter, P. Michler, C. Roy, and S. Hughes, *Phys. Rev. B* **86**, 241304(R) (2012).
- [50] A. Kuhn, M. Hennrich, and G. Rempe, *Phys. Rev. Lett.* **89**, 067901 (2002).
- [51] T. Grange, N. Somaschi, C. Antón, L. De Santis, G. Coppola, V. Giesz, A. Lemaitre, I. Sagnes, A. Auffèves, and P. Senellart, *Phys. Rev. Lett.* **118**, 253602 (2017).
- [52] P. Borri, W. Langbein, S. Schneider, U. Woggon, R. L. Sellin, D. Ouyang, and D. Bimberg, *Phys. Rev. Lett.* **87**, 157401 (2001).
- [53] Y. Ota, S. Iwamoto, N. Kumagai, and Y. Arakawa, [arXiv:0908.0788](https://arxiv.org/abs/0908.0788).
- [54] A. Reigues, J. Iles-Smith, F. Lux, L. Monniello, M. Bernard, F. Margailan, A. Lemaitre, A. Martinez, D. P. S. McCutcheon, J. Mørk, R. Hosten, and V. Voliotis, *Phys. Rev. Lett.* **118**, 233602 (2017).
- [55] H. Wang, Z.-C. Duan, Y.-H. Li, S. Chen, J.-P. Li, Y.-M. He, M.-C. Chen, Y. He, X. Ding, C.-Z. Peng, C. Schneider, M. Kamp, S. Höfling, C.-Y. Lu, and J.-W. Pan, *Phys. Rev. Lett.* **116**, 213601 (2016).
- [56] A. Muller, E. B. Flagg, P. Bianucci, X. Y. Wang, D. G. Deppe, W. Ma, J. Zhang, G. J. Salamo, M. Xiao, and C. K. Shih, *Phys. Rev. Lett.* **99**, 187402 (2007).
- [57] S. Ates, S. M. Ulrich, S. Reitzenstein, A. Löffler, A. Forchel, and P. Michler, *Phys. Rev. Lett.* **103**, 167402 (2009).
- [58] A. N. Vamivakas, Y. Zhao, C.-Y. Lu, and M. Atatüre, *Nat. Phys.* **5**, 198 (2009).
- [59] G. Cui and M. G. Raymer, *Phys. Rev. A* **73**, 053807 (2006).
- [60] B. R. Mollow, *Phys. Rev.* **188**, 1969 (1969).
- [61] N. V. Vitanov, A. A. Rangelov, B. W. Shore, and K. Bergmann, *Rev. Mod. Phys.* **89**, 015006 (2017).
- [62] E. Knill, *Nature (London)* **434**, 39 (2005).
- [63] Y.-J. Wei, Y.-M. He, M.-C. Chen, Y.-N. Hu, Y. He, D. Wu, C. Schneider, M. Kamp, S. Höfling, C.-Y. Lu, and J.-W. Pan, *Nano Lett.* **14**, 6515 (2014).